Journal of Power Sources 195 (2010) 6486–6490

Contents lists available at ScienceDirect

Journal of Power Sources

journal homepage: www.elsevier.com/locate/jpowsour

Short communication

Electrical properties of grain boundaries and size effects in samarium-doped ceria

Duanting Yan[a], Xiaomei Liu[a,*], Xinyu Bai[b], Li Pei[a], Minzhang Zheng[a], Chengjun Zhu[a], Dejun Wang[a], Wenhui Su[a]

[a] State Key Laboratory of Superhard Materials, Department of Physics, Jilin University, Jiefang Road, Changchun 130023, PR China
[b] Jilin Science and Technology Museum, Renming Street, Changchun 130021, PR China

ARTICLE INFO

Article history:
Received 16 February 2010
Received in revised form 11 April 2010
Accepted 12 April 2010
Available online 24 April 2010

Keywords:
Doped ceria
Apparent specific grain-boundary conductivity
Siliceous phase
Space-charge potential
Solid oxide fuel cells

ABSTRACT

$Ce_{0.85}Sm_{0.15}O_{1.925}$ samples have been prepared using the glycine-nitrate process. The effects of microstructure on their electrical properties were investigated by X-ray diffraction, density measurements, scanning electron microscopy and AC impedance spectroscopy. The grain-boundary conductivities and total conductivities increase with decreasing grain size for sintered densities of 95% or greater. The bulk conductivities are nearly independent of grain size for sintered densities of 95% or greater. It is found that the space-charge potential is nearly independent of grain size and the increase of the conduction path width is responsible for the increase of the apparent specific grain-boundary conductivity. The power densities and current densities of single cells based on $Ce_{0.85}Sm_{0.15}O_{1.925}$ electrolytes with different grain size are evaluated.

1. Introduction

In recent years, a solid oxide fuel cell (SOFC) that operates at lower temperatures (500–700 °C) has been of particular interest, mainly because it has the advantage of reducing costs by removing constraints on the type of materials (e.g. ceramics) constituting the SOFC system [1–3]. Ceria-based solid solutions have been considered as promising electrolytes for intermediate temperature (600–800 °C) solid oxide fuel cells (IT-SOFCs) due to their excellent oxygen-ion conductivity compared to yttria-stabilized zirconia (YSZ). Acceptor-doped CeO_2 is present in the form of polycrystals, so the grain boundaries often have a significant influence on the overall properties. In the low temperature regime, the specific grain-boundary conductivity is known to be 2–3 orders lower than the bulk conductivity [4–6]. To improve the grain-boundary conductivity σ_{gb} of acceptor-doped CeO_2, the influence of grain size on σ_{gb} has been investigated [7–10]. However, the effects of grain size on σ_{gb} are divergent.

In this communication, we present AC impedance measurements on acceptor-doped CeO_2 samples with different grain sizes and the size effects are observed. A novel method to analyse the grain-boundary transport in acceptor-doped CeO_2 of normal purity is presented, and the origin of the grain size effects for acceptor-doped CeO_2 is investigated. The power densities and current densities of single cells based on $Ce_{0.85}Sm_{0.15}O_{1.925}$ electrolytes with different grain sizes are evaluated.

2. Experimental

$Ce_{0.85}Sm_{0.15}O_{1.925}$ powders were prepared by the glycine-nitrate process [11] and calcined in air at 600 °C for 6 h to remove any carbon residues remaining in the oxide powder. Then the powders were ground and cold pressed at a pressure of about 300Mpa to obtain green compact pellets with a thickness of ~0.5 mm and diameter of ~13.6 mm using a uniaxial die press. Then the $Ce_{0.85}Sm_{0.15}O_{1.925}$ pellets were sintered in air at 1150, 1250, 1350 and 1450 °C for 10 h.

The power densities and current densities of single cells based on the $Ce_{0.85}Sm_{0.15}O_{1.925}$ electrolytes with different grain size were evaluated. The $Ni_{0.9}Cu_{0.1}O_x$ and $Ce_{0.85}Sm_{0.15}O_{1.925}$ oxide powders were prepared by the glycine-nitrate process as described elsewhere [11]. The $Ni_{0.9}Cu_{0.1}O_x$ and $Ce_{0.85}Sm_{0.15}O_{1.925}$ powders thus obtained were mixed in the weight ratio 60:40 and ball-milled for 12 h in ethanol to obtain the anode powders. The $BaCo_{0.7}Fe_{0.2}Nb_{0.1}O_{3-\delta}$ oxide powders were prepared by a conventional solid state reaction process [3]. The $Ce_{0.85}Sm_{0.15}O_{1.925}$ electrolyte disks were polished to reduce the thickness to 360 μm. $Ni_{0.9}Cu_{0.1}O_x$–$Ce_{0.85}Sm_{0.15}O_{1.925}$ and

* Corresponding author. Tel.: +86 431 85172529; fax: +86 431 85172529.
E-mail address: xiaomeiliu58@sina.com (X. Liu).

0378-7753/$ – see front matter © 2010 Elsevier B.V. All rights reserved.
doi:10.1016/j.jpowsour.2010.04.034

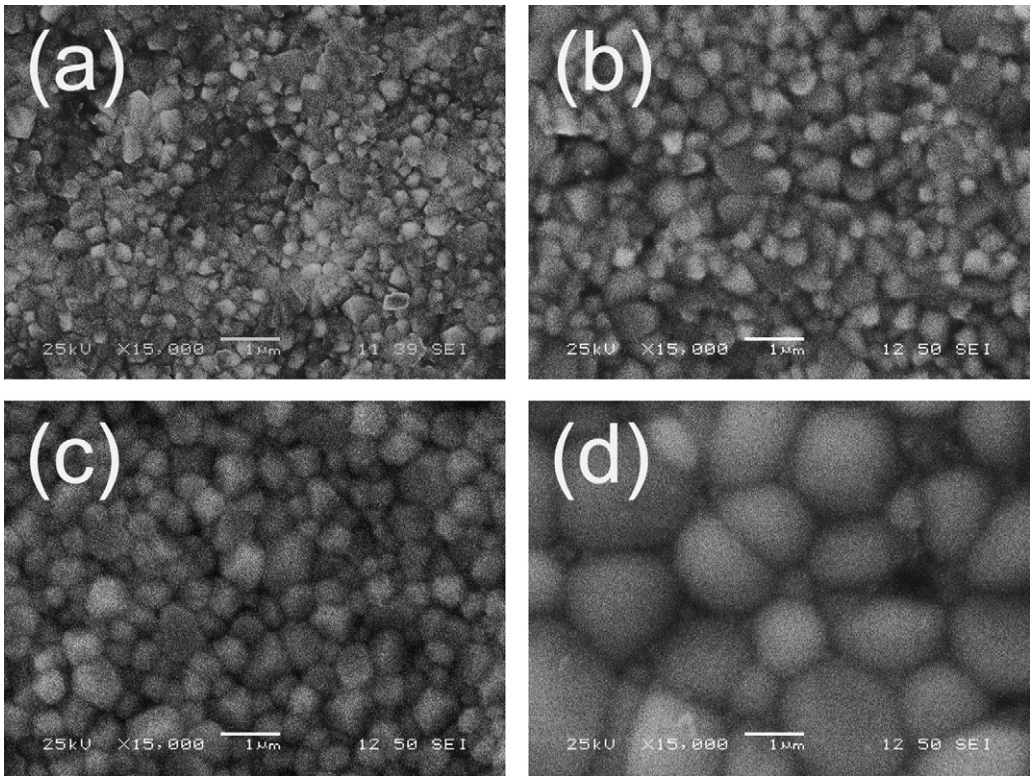

Fig. 1. Microstructure of $Ce_{0.85}Sm_{0.15}O_{1.925}$ sintered at (a) 1150 °C, (b) 1250 °C, (c) 1350 °C, and (d) 1450 °C for 10 h.

$BaCo_{0.7}Fe_{0.2}Nb_{0.1}O_{3-\delta}$ were made into inks with ethyl cellulose and terpineol. $Ni_{0.9}Cu_{0.1}O_x$–$Ce_{0.85}Sm_{0.15}O_{1.925}$ ink was screen printed onto one side of the $Ce_{0.85}Sm_{0.15}O_{1.925}$ disk followed by sintering at 1000 °C for 5 h. $BaCo_{0.7}Fe_{0.2}Nb_{0.1}O_{3-\delta}$ cathode ink was subsequently painted onto the other side of the $Ce_{0.85}Sm_{0.15}O_{1.925}$ disk and sintered at 1000 °C for another 2 h. Silver paste was applied to the anode and cathode surfaces to serve as current collectors, followed by attachment of two silver wires to each electrode to serve as current and voltage leads. The single cell made in this way was sealed onto one end of an alumina tube with silver paste.

The phase of $Ce_{0.85}Sm_{0.15}O_{1.925}$ sintered in air at 1150, 1250, 1350, and 1450 °C for 10 h was confirmed by X-ray diffraction to have the fluorite structure. The microstructure was investigated by means of a scanning electron microscope (SEM, JSM-6480LV, JEOL, Japan) and the average grain sizes d_g were estimated using the linear intercept method by randomly selecting more than 250 grains from the SEM micrographs. The densities of the sintered pellets were measured using the Archimedes method. The electrical conductivity of the materials was measured using the sintered ceramic pellets. Silver paste was used as electrodes on opposite sides of each tablet, with an electrode area of ~0.25 cm^2. Impedance measurements of the sintered pellets were conducted in air over the temperature range 300–800 °C, and frequency range 0.1–10^6 Hz at an amplitude of 10 mV with a Solartron 1260 frequency response analyzer. The single cell performance was tested at temperatures from 500 to 800 °C with a Solartron SI 1287 electrochemical interface, using hydrogen (100 ml min^{-1}) as the fuel on the anode side and air as the oxidant on the cathode side.

3. Results and discussion

Fig. 1 shows SEM micrographs of the $Ce_{0.85}Sm_{0.15}O_{1.925}$ ceramics sintered at different temperatures. All samples exhibit a homogeneous structure. The relative density and grain size of the $Ce_{0.85}Sm_{0.15}O_{1.925}$ ceramics are presented in Table 1. Samples with over 95% relative density can be obtained after sintering at a temperature higher than 1250 °C for 10 h.

Typical impedance spectra are shown in Fig. 2. In the order of decreasing frequency, arcs corresponding to the responses of the grain bulk, the grain boundaries and the electrodes, respectively, were recorded. The quantitative change of the bulk and grain-boundary conductivities in the temperature range 300–500 °C were obtained by fitting these impedance plots using a software package. Bulk conductivities, grain-boundary conductivities and total conductivities as a function of average grain size for $Ce_{0.85}Sm_{0.15}O_{1.925}$ samples at 400 °C are shown in Fig. 3.

The temperature dependence of the bulk conductivity σ_{bulk}, the grain-boundary conductivity σ_{gb} and total conductivity σ_{tot} are presented in Fig. 4. The grain-boundary conductivity is $\sigma_{gb} = L/AR_{gb}$,

Table 1
Sintering conditions, relative density, average grain size (d_g) and activation energies for bulk and grain-boundary conductivities (E_α^{bulk} and E_α^{gb}).

Sintering condition	Relative density (%)	d_g (nm)	E_α^{bulk} (eV)	E_α^{gb} (eV)	$E_\alpha^{gb} - E_\alpha^{bulk}$ (eV)
1150 °C × 10 h	92.4 ± 0.2	260	0.65 ± 0.01	1.02 ± 0.01	0.37
1250 °C × 10 h	95.2 ± 0.1	320	0.67 ± 0.01	1.02 ± 0.02	0.35
1350 °C × 10 h	95.1 ± 0.1	580	0.67 ± 0.01	1.01 ± 0.01	0.34
1450 °C × 10 h	96.2 ± 0.1	1680	0.65 ± 0.01	0.99 ± 0.01	0.34

Activation energies for bulk (E_α^{bulk}) and grain-boundary (E_α^{gb}) conductivities were taken in the temperature range of 300–500 °C in air.

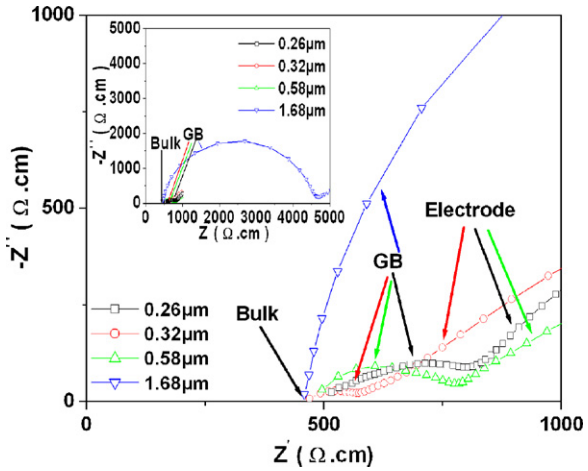

Fig. 2. Impedance spectra at 400 °C for $Ce_{0.85}Sm_{0.15}O_{1.925}$ samples with average grain sizes of 0.26 μm, 0.32 μm, 0.58 μm and 1.68 μm, respectively.

with R_{gb} being the grain-boundary resistance of the samples, where L is the sample thickness and A is the electrode area on the sample surface. In this way, the bulk conductivity σ_{bulk} and total conductivity σ_{tot} can be obtained. As shown in Figs. 3 and 4, σ_{bulk} is nearly independent of the grain size d_g, but σ_{gb} and σ_{tot} increase with decreasing grain size d_g for samples sintered at 1250, 1350 and 1450 °C. The bulk conductivity σ_{bulk} of the $Ce_{0.85}Sm_{0.15}O_{1.925}$ sintered at 1150 °C is lower than the others. Lower sintered densities produce a small decrease in the bulk conductivity when the relative density is below 95% [12], and the decrease of σ_{bulk} is probably due to the bulk "de-doping" resulting from the grain size-dependent grain-boundary segregation [4]. The grain-boundary conductivity σ_{gb} of $Ce_{0.85}Sm_{0.15}O_{1.925}$ sintered at 1150 °C are lower than for samples sintered at 1250 and 1350 °C. Lower sintered densities produce a large decrease in grain-boundary conductivity when the relative density is below 95% [12]. The reason that the values of σ_{gb} increase with decreasing grain size d_g for samples sintered at 1250, 1350 and 1450 °C and the σ_{gb} of $Ce_{0.85}Sm_{0.15}O_{1.925}$ sintered at 1450 °C is lower than the sample sintered at 1150 °C can be explained as follows.

From a structural point of view, a grain boundary is a crystallographic mismatch zone (i.e. grain-boundary core). At thermodynamic equilibrium, the grain-boundary core of $Ce_{0.85}Sm_{0.15}O_{1.925}$ carries an electrical charge due to the presence of excess oxygen vacancies. This charge is compensated by adjacent space

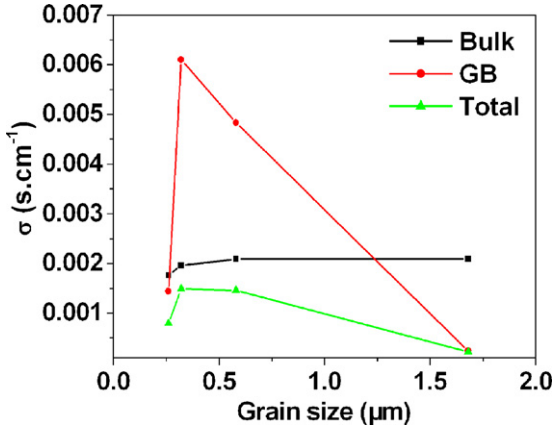

Fig. 3. Bulk conductivities, grain-boundary conductivities and total conductivities as a function of average grain size for $Ce_{0.85}Sm_{0.15}O_{1.925}$ samples at 400 °C.

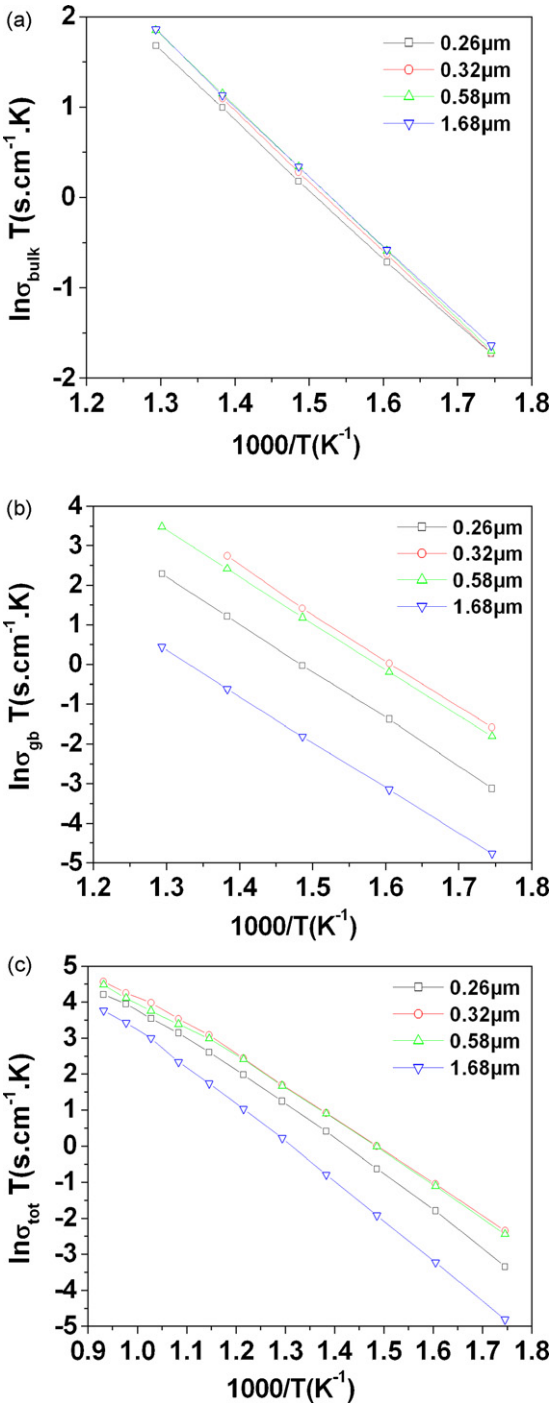

Fig. 4. Temperature dependences of (a) bulk conductivities, (b) grain-boundary conductivities, and (c) total conductivities for $Ce_{0.85}Sm_{0.15}O_{1.925}$ samples with average grain sizes of 0.26 μm, 0.32 μm, 0.58 μm and 1.68 μm.

charges of the Sm'_{Ce}. An electrostatic potential $\Delta\varphi(x)$ between the grain-boundary and the bulk can be present [5,13,14]. The grain-boundary conductivity, controlled by the space charge $\sigma(x)$, is given as [14]

$$\sigma(x) = \sigma_{bulk} \exp\left(-\frac{2e\Delta\varphi(x)}{k_B T}\right) \quad (1)$$

where x is the distance from the interface between the grain-boundary core and the space-charge layer (Fig. 5(b)), $\sigma(x)$ is the conductivity at x, σ_{bulk} is the bulk conductivity, e is the elemen-

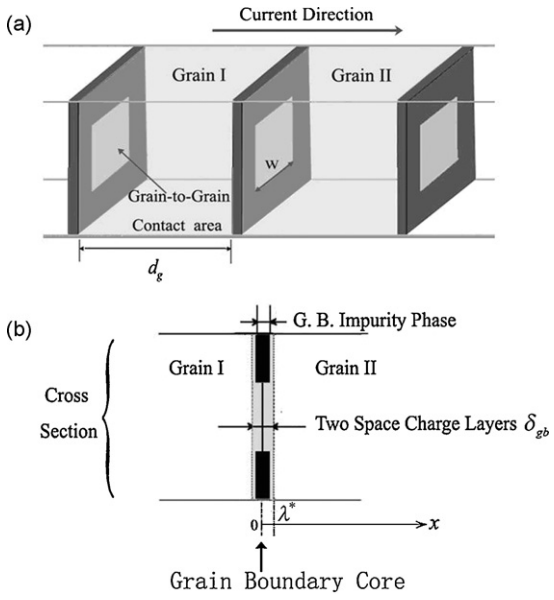

Fig. 5. (a) Three-dimensional schematic representation and (b) cross-section of grain boundaries and grain-boundary conduction pathways (similar to Fig. 6 in [14]).

tary charge, k_B is the Boltzmann constant and T is the absolute temperature.

For high-purity materials (usually <50 ppm SiO_2), grain-boundary behavior is usually attributed to the effect of intrinsic space-charge layers. However, even a few hundred ppm of a siliceous impurity could increase the grain-boundary resistivity of $Ce_{0.8}Gd_{0.2}O_{2-\delta}$ by up to 100 times [6], and most materials used to date contain several hundreds ppm of SiO_2 impurity [7], so the apparent specific grain-boundary conductivity cannot be attributed solely to the effect of space-charge layers only [7] and the impurity factor must be taken into consideration.

For normal purity materials, the grain-boundary conduction pathway can be schematically represented by Fig. 5, by assuming the grain is cubic, the grain size is d_g, the direct grain-to-grain contact area is square and the side length is ω, giving the area of grain-to-grain contact ω^2.

Because the ionic transport across the grain boundaries occurs solely through grain-to-grain contacts [4–5,14], the resistance of a grain boundary should be equal to the resistance of two space-charge layers of area ω^2,

$$\langle R_{gb}\rangle = 2\sum \frac{1}{\sigma(x)}\frac{\Delta x}{\omega^2} = \frac{2}{\omega^2\sigma_{bulk}}\int_0^{\lambda^*}\exp\left(\frac{2e\Delta\varphi(x)}{k_BT}\right)dx \quad (2)$$

with λ^* being the width of the space-charge layer.

On the other hand, the apparent resistance of a grain boundary is as follows

$$\langle R_{gb}\rangle = \frac{1}{\sigma_{gb}^{as}}\frac{2\lambda^*}{d_g^2} \quad (3)$$

with σ_{gb}^{as} being the apparent specific grain-boundary conductivity, which is an experimental datum and can be calculated from $\sigma_{gb}^{as} = L\delta_{gb}/AR_{gb}d_g$ [4–5,14], where δ_{gb} is the grain-boundary thickness, L the sample thickness, A the electrode area on the samples surface and R_{gb} the grain-boundary resistance from AC impedance spectra. The bulk resistance of the same size is

$$\langle R_{bulk}\rangle = \frac{1}{\sigma_{bulk}}\frac{2\lambda^*}{d_g^2} \quad (4)$$

Hence

$$\frac{\sigma_{gb}^{as}}{\sigma_{bulk}} = \frac{\langle R_{bulk}\rangle}{\langle R_{gb}\rangle} = \frac{\omega^2}{d_g^2}\left(\frac{1}{\lambda^*}\int_0^{\lambda^*}\exp\left(\frac{2e\Delta\varphi(x)}{k_BT}\right)dx\right)^{-1} = \frac{\omega^2}{d_g^2}\frac{4e\Delta\varphi(0)}{k_BT}\exp\left(-\frac{2e\Delta\varphi(0)}{k_BT}\right) \quad (5)$$

In Eq. (5), $\Delta\varphi(0) = \varphi(0) - \varphi(\infty)$, and is the potential of the grain-boundary core relative to the bulk [14]. The $(\omega/d_g)^2$ term is called the "impurity blocking term", and results from the effect of decreasing the conduction path width by an impurity. Obviously, the $(\omega/d_g)^2$ term represents the clean fraction of resistive siliceous films at the grain boundaries, and is dependent on the purity and grain size of the sample. The relocation of the siliceous phase is impossible below 800 °C [15], so the value of $(\omega/d_g)^2$ should be independent of the testing temperature in the range 300–800 °C. The $\sigma_{gb}^{as}/\sigma_{bulk}$ term represents the blocking effect of the grain boundary.

The activation energy, E_α, is defined as $E_\alpha = -1000k_B[d\ln(\sigma T)/d(1000/T)]$. Accordingly, differentiating Eq. (5) yields

$$E_\alpha^{gb} - E_\alpha^{bulk} = (2e\Delta\varphi(0) - k_BT)\left[1 + \left[\frac{1}{T}\Delta\varphi(0)\right]\frac{d\Delta\varphi(0)}{d(1/T)}\right] \quad (6)$$

The $e\Delta\varphi(0)$ in Eq. (6) is the energy required to transfer oxygen vacancies from the bulk to the grain-boundary space-charge region [14,16]. As shown in Table 1, the value of $E_\alpha^{gb} - E_\alpha^{bulk}$ is almost independent of d_g, which agrees well with reported results [4,7,14]. From Eq. (6), $\Delta\varphi(0)$ should be nearly independent of d_g.

The apparent specific grain-boundary conductivity σ_{gb}^{as} can be expressed as $\sigma_{gb}^{as} = \sigma_{gb}\delta_{gb}/d_g$, because the σ_{gb} increase with decreasing grain size d_g (shown in Fig. 3 and Fig. 4(b)). Also, the value of δ_{gb}/d_g increases with decreasing grain size d_g, so the σ_{gb}^{as} increase with decreasing grain size d_g for sintered densities of 95% or greater. Because σ_{bulk} is nearly independent of the grain size d_g (shown in Fig. 3 and Fig. 4(a)), the $\sigma_{gb}^{as}/\sigma_{bulk}$ increase with decreasing grain size d_g for sintered densities of 95% or greater. Because $\Delta\varphi(0)$ is nearly independent of d_g, from Eq. (5), the increase of $\sigma_{gb}^{as}/\sigma_{bulk}$ should result from the increase of $(\omega/d_g)^2$ with decreasing grain size d_g. Finer grain size provides large grain-boundary areas upon which impurities can precipitate [5], so the grain-to-grain contact area $(\omega/d_g)^2$ increased with decreasing grain size d_g. Although the relative density of $Ce_{0.85}Sm_{0.15}O_{1.925}$ sintered at 1450 °C is higher than that of the sample sintered at 1150 °C, a high sintering temperature (1450 °C) leads to an obvious increase in the grain size, which provides very small grain-boundary areas for impurities to precipitate, as well as a change in the viscosity and wetting nature of the GB phase, which promotes the propagation of impurities along the grain boundaries. Both factors result in a decrease of the GB clean fraction [7]. According, σ_{gb} of $Ce_{0.85}Sm_{0.15}O_{1.925}$ sintered at 1450 °C is lower than the sample sintered at 1150 °C.

Fig. 6 shows plots of the performance of various single fuel cells using $Ce_{0.85}Sm_{0.15}O_{1.925}$, with different grain size, as electrolytes at 800 °C. It can be seen that the power densities and current densities of single cells increase with decrease of the grain size of $Ce_{0.85}Sm_{0.15}O_{1.925}$ electrolytes for sintered densities of 95% or greater, and then decrease for the sample sintered at 1150 °C. The maximum power densities of the cells are 498, 648, 573 and 468 mW cm^{-2} at 800 °C for $Ce_{0.85}Sm_{0.15}O_{1.925}$ sintered at 1150, 1250, 1350 and 1450 °C for 10 h, respectively.

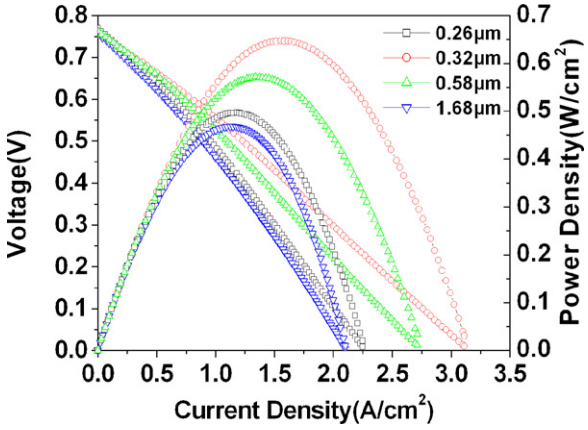

Fig. 6. Performance of cells ($BaCo_{0.7}Fe_{0.2}Nb_{0.1}O_{3-\delta}$/$Ce_{0.85}Sm_{0.15}O_{1.925}$/$Ni_{0.9}Cu_{0.1}O_x$–$Ce_{0.85}Sm_{0.15}O_{1.925}$) with $Ce_{0.85}Sm_{0.15}O_{1.925}$ sintered at different temperatures as electrolytes at 800 °C. Hydrogen and ambient air were used as the fuel and oxidant, respectively.

4. Conclusions

The grain-boundary conductivity and total conductivity increased with decreasing grain size for sintered densities of 95% or greater. The space-charge potential was nearly independent of grain size. The increase of the apparent specific grain-boundary conductivity resulted from the increase of the conduction path width determined by the siliceous phase at the grain boundaries. The power densities and current densities of single cells increase with decreasing grain size of $Ce_{0.85}Sm_{0.15}O_{1.925}$ electrolytes for sintered densities of 95% or greater.

Acknowledgements

This work was supported by the National Natural Science Foundation of China (no. 50872041), and by the National Foundation for Fostering Talent in Basic Science of China (no. J0730311), and the Foundation of State Key Laboratory of Superhard Materials (200908).

References

[1] C.J. Zhu, X.M. Liu, D. Xu, D.J. Wang, D.T. Yan, L. Pei, T.Q. Lü, W.H. Su, J. Power Sources 185 (2008) 212–216.
[2] C.J. Zhu, X.M. Liu, C.S. Yi, D.T. Yan, W.H. Su, J. Power Sources 185 (2008) 193–196.
[3] C.J. Zhu, X.M. Liu, C.S. Yi, L. Pei, D.T. Yan, J.P. Niu, D.J. Wang, W.H. Su, Electrochem. Commun. 11 (2009) 958–961.
[4] X. Guo, Z.L. Zhang, Acta Mater. 51 (2003) 2539–2547.
[5] C.Y. Tian, S.W. Chan, Solid State Ionics 134 (2000) 89–102.
[6] Y.H. Cho, P.S. Cho, G. Auchterlonie, D.K. Kim, J.H. Lee, D.Y. Kim, H.M. Park, J. Drennan, Acta Mater. 55 (2007) 4807–4815.
[7] T.S. Zhang, J. Ma, Y.Z. Chen, L.H. Luo, L.B. Kong, S.H. Chan, Solid State Ionics 177 (2006) 1227–1235.
[8] D. Perez-Coll, P. Nunez, J.C.C. Abrantes, D.P. Fagg, V.V. Kharton, J.R. Frade, Solid State Ionics 176 (2005) 2799–2805.
[9] X.Q. Sha, Z. Lü, X.Q. Huang, J.P. Miao, Z.G. Liu, X.S. Xin, Y.H. Zhang, W.H. Su, J. Alloys Compd. 433 (2007) 274–278.
[10] V. Gil, J. Tartaj, C. Moure, P. Duran, J. Eur. Ceram. Soc. 26 (2006) 3161–3171.
[11] D.T. Yan, X.M. Liu, D. Xu, C.J. Zhu, W.G. Ma, J.B. Niu, Y.X. Liu, W.H. Su, Solid State Ionics 179 (2008) 995–999.
[12] I.R. Gibson, G.P. Dransfield, J.T.S. Irvine, J. Mater. Sci. 33 (1998) 4297–4305.
[13] A. Tschope, Solid State Ionics 139 (2001) 267–280.
[14] X. Guo, R. Waser, Prog. Mater. Sci. 51 (2006) 151–210.
[15] S.P.S. Badwal, Solid State Ionics 76 (1995) 67–80.
[16] T. Van Dijk, A.J. Burggraaf, Phys. Stat. Sol. A 63 (1981) 229–240.